Title: HIV-1 Vpr accessory protein interacts with REAF and mitigates its associated anti-viral activity.

Short title: Vpr mitigates REAF

Authors: Joseph M Gibbons[1], Kelly M Marno[1], Rebecca Pike[1], Wing-yiu Jason Lee[1], Christopher E Jones[1], B. W. Ogunkolade[1], Claire Pardieu[1], Gary Warnes[1], Paul A Rowley[2], Richard D Sloan[3,4] and Áine McKnight[1]

Abstract: The accessory protein Vpr of Human Immunodeficiency Virus type 1 (HIV-1) enhances replication of the virus in macrophages (1-7). Virus particle packaged Vpr is released in target cells shortly after entry, suggesting it is required early in infection (8, 9). Why it is required for infection of macrophages and not cycling T-cells and why it induces G2/M arrest in cycling cells are unknown. Here we observe, by co-immunoprecipitation assay, an interaction between Vpr and endogenous REAF (RNA-associated Early-stage Antiviral Factor, RPRD2), a protein shown previously to potently restrict HIV infection(10). After HIV-1 infects macrophages, within 30 minutes of viral entry, Vpr induces the degradation of REAF. Subsequently, as replication continues, REAF expression is upregulated – a response which is curtailed by Vpr. REAF is more highly expressed in differentiated macrophages than in cycling T-cells. Expression in cycling cells is cell-cycle dependent and knockdown induces cell-cycle perturbation. Therefore, our results support the long held hypothesis that Vpr induces the degradation of a factor involved in the cell cycle that impedes HIV infection in macrophages.

[1]The Blizard Institute, Queen Mary University of London School of Medicine and Dentistry, QMUL, UK. [2]Department of Biological Sciences, The University of Idaho, Moscow, Idaho, USA. [3]Division of Infection and Pathway Medicine, The University of Edinburgh, UK. [4]ZJU-UoE Institute, Zhejiang University, P.R. China.

Summary

Human Immunodeficiency Virus type 1 (HIV-1) has so called accessory proteins which modulate the activity of host proteins, enabling efficient replication of the virus. The precise function of one such accessory protein, Vpr, has so far not been revealed. REAF is a host protein that limits the capacity of HIV-1 to infect cells. Here, we show that Vpr interacts with REAF. Shortly after infection, only when Vpr is present, REAF is degraded in primary macrophages. Vpr further curtails the cells subsequent increase in REAF production. Additionally, when the ability of cell to produce REAF is prevented, the population accumulates in the G2/M phase of the cell cycle. In infection, Vpr sends cells into G2/M arrest. This study therefore supports the long held hypothesis that Vpr is responsible for the degradation of a cellular factor involved in the cell cycle and one which impedes the completion of HIV-1 replication.

Introduction

Human Immunodeficiency Virus type 1 (HIV-1) infects $CD4^+$ T-cells and macrophages *in vivo* and causes Acquired Immunodeficiency Syndrome (AIDS). HIV-1 has four non-structural accessory genes *nef*, *vif*, *vpu* and *vpr* that mitigate host innate immunity. A function for Vpr has been elusive, but it is required for replication in macrophages and for pathogenesis *in vivo* (1, 2). Substantial amounts are incorporated into viral particles and released from the major capsid protein (CA) after entry into the cell (8, 9). Concurrently, reverse transcription transcribes the RNA genome into DNA, which integrates into the host cell DNA. It is released early from the CA (11) suggesting it has an early function up to integration. Here we show that within 30 minutes of cellular entry, Vpr containing virus induces the degradation of RNA-associated Early-stage Antiviral Factor (REAF, also known as RPRD2). REAF, formerly described as Lv2, limits the

46 completion of pro-viral DNA synthesis and integration (10).

47

48 **Results and Discussion**

49 HeLa-CD4, knocked down for REAF (HeLa-CD4 shRNA-REAF, Figure 1A), [10], were
50 challenged with HIV-1 89.6^{WT} or virus deleted for *vpr* ($89.6^{\Delta vpr}$), *vif* ($89.6^{\Delta vif}$) or *vpu* ($89.6^{\Delta vpu}$).
51 Figure 1B shows that despite a standard virus input (50 FFU/ml as measured on HeLa-CD4), the
52 removal of REAF using shRNA alleviates the need for Vpr. There is significantly greater rescue
53 of HIV-1 $89.6^{\Delta vpr}$ (>60 fold, $p<0.0001$) compared to HIV-1 89.6^{WT} or virus lacking *vpu* or *vif* (20
54 fold). Thus *vpr* overcomes REAF restriction.

55 REAF is transiently knocked down in HeLa-CD4 shortly after HIV-1 infection (12). Here,
56 HeLa-CD4 infected with HIV-1 89.6^{WT} or HIV-1 $89.6^{\Delta vpr}$ were quantified for REAF nuclear or
57 cytoplasmic protein over time by imaging flow cytometry. Following infection with HIV-1
58 $89.6^{\Delta vpr}$, REAF levels increase in both the nucleus (~25%, Figure 1C) and cytoplasm (~10%,
59 Figure 1D) within 30 minutes with nuclear levels remaining high for 180 minutes. In the presence
60 of Vpr (HIV-1 89.6^{WT}) however this increase in REAF is curtailed at 30 minutes, with a steady
61 decline as time progresses. The decline is most marked in the nucleus with ~20% reduction by 60
62 minutes and ~30% at 120 minutes. By 180 minutes, levels of REAF recover.

63 Imaging flow cytometry software determined the 'nuclear enrichment score' over time
64 after infection with HIV-1 89.6^{WT} or HIV-1 $89.6^{\Delta vpr}$ (Figure 1E). The lower the score the less
65 REAF in the nucleus relative to in the cell overall. By 60-120 minutes, a significant ($p<0.05$)
66 segregation emerges. In the presence of Vpr, relative nuclear levels of REAF are suppressed
67 between 30 and 120 minutes ($p<0.05$). Lower levels of REAF were also observed in the cytoplasm
68 over time but to a much lesser extent. The virus carries limited quantities of Vpr (11), potentially

explaining why REAF levels return to normal or above by 180 minutes. Our results support the current model for Vpr activity - it interacts with the cullin4A-DDB1 (DCAF1) E3 ubiquitin ligase and induces proteasomal degradation of an unknown substrate (13). We reported that REAF is degraded by the proteasome by HIV-1 infection in HeLa-CD4 (12) consistent with these observations. Furthermore, Figure 1F shows that Vpr and REAF interact with each other, either directly or as part of a complex, as they are co-immunoprecipitated. This supports our proposition that Vpr induces the degradation of REAF.

Other targets of Vpr have been proposed. It recruits SLX4-SLX1/MUS81-EME1 endonucleases to DCAF1, activating MUS81 degradation and triggering arrest in G2/M (14). It also degrades helicase-like transcription factor (HLTF) (15). We show here both HLTF (Figure 1G) and MUS81 (Figure 1H) are depleted by virus concomitantly with REAF within 60 minutes of infection. Interestingly, HLTF and REAF were identified in the same screen for proteins that interact with single-stranded DNA (16). We previously showed that REAF binds cellular and viral DNA and viral DNA-containing reverse transcripts (12). The depletion of REAF after infection is transient, with the recovery by 120 minutes likely reflecting the limited quantities of Vpr carried in the virus particle(11). In contrast, HLTF and MUS81 levels remain diminished for at least 48 hours suggesting they have a role later in virus life cycle (*27*, *22*). Unlike REAF, neither SLX4-MUS81-EME1 nor HLTF have so far been directly linked with HIV-1 restriction (17).

We defined the cell cycle phase (G1/0, S and G2/M) of primary human monocytes and analysed REAF expression. Levels are lowest in G1, increase through S phase, and peak in G2/M (Figure 2A). REAF levels during the cell cycle were further followed after synchronization at the G2/M border (Figure 2B, Figure S1). When synchronised cells cycled from G2 into M, REAF levels declined but recovered after 8 hours. The major decline in REAF expression coencides with

92 phosphorylation of histone H3 (Ser10/Thr11), a mitotic cell marker (Figure 2B) (18).

93 Using imaging flow cytometry we further analysed the subcellular localisation of REAF
94 during mitosis (Figure 2C). An asynchronous population had a nuclear enrichment score of 0.92.
95 Nocodazole-treated cells diverged into two populations: one with a low score (0.13) and another
96 with a high score (1.53) (Figure 2C, left). Phospho-histone H3 (Ser28) staining confirmed cells in
97 mitosis had a low score of 0.17, and thus lower levels of REAF in the nucleus relative to the cell
98 overall (Figure 2C, right and 2D). Using confocal microscopy, REAF is observed in both the
99 cytoplasm and nucleus through interphase, prophase and prometaphase but excluded from
100 chromatin during metaphase, anaphase and telophase (Figure 2E). Furthermore, down modulation
101 of REAF in HeLa-CD4 shRNA-REAF induces accumulation of cells at G2/M (Figure 2F). Flow
102 cytometry of DNA content in PI stained cells shows they accumulated (25%) in G2/M compared
103 to parental (14%).

104 Vpr has been shown to varying degrees to be more beneficial for replication in
105 macrophages than in cycling T-cells *(3-7)*. We compared the susceptibility of mitotic HeLa-CD4
106 (92.5%) to an asynchronous population (2.6% mitotic, Figure 3A) using HIV-1 89.6 (VSV-G) with
107 a GFP reporter as challenge virus. Mitotic cells were 12 fold more susceptible (Figure 3B). This
108 was confirmed using HIV-1 89.6^{WT} expressing HIV-1 envelope (Figure S2). Thus REAF exclusion
109 from chromatin during mitosis may provide an opportunity to evade restriction in cycling T-cells.
110 The results concur with previous reports suggesting cell cycle arrest in G2/M promotes early HIV-
111 1 infection (19) and that there is delayed replication kinetics of *vpr* mutants in T-cells (20). Figure
112 1 C-D above suggested that nuclear intensity of REAF is key to HIV restriction. We measured
113 expression of REAF in the nucleus of resting or activated $CD4^+$ T-cells, monocytes or
114 macrophages and dendritic cells (DC) (Figure 3C). Expression levels are higher in MDMs

compared to T-cells again concurring with the need for HIV-1 Vpr to infect macrophages but not T-cells. The differential expression of REAF protein in monocytes and MDMs was confirmed by Western blotting (Figure 3D).

Antiviral factors are often upregulated in response to pathogen associated molecular patterns. Polyriboinosinic:polyribocytidylic acid (poly(I:C)) is a double-stranded RNA, used to stimulate viral infection associated molecular pattern recognition pathways. Figure 3E shows poly(I:C) induction of REAF in THP-1, a macrophage cell line.

To decipher a role for Vpr and REAF in primary macrophages, MDMs were challenged with either HIV-1 89.6^{WT} or HIV-1 $89.6^{\Delta vpr}$. Western blot analysis shows that REAF levels decline within 30 and up to 60 minutes of challenge with HIV-1 89.6^{WT} (Figure 3F). Basal levels return by 240 minutes. This contrasts with HIV-1 $89.6^{\Delta vpr}$ infection where REAF levels do not decline and indeed rise from 60 to 240 minutes (Figure 3G). Thus, MDMs respond to HIV-1 infection by upregulating REAF, but Vpr mitigates this by inducing REAF's degradation.

The subcellular fluctuation of REAF levels in MDMs after challenge with HIV-1 89.6^{WT} or HIV-1 $89.6^{\Delta vpr}$ was determined using imaging flow cytometry. With Vpr, nuclear REAF decreases between 60 and 120 minutes ($P < 0.05$, Figure 3H), similar to HeLa-CD4. In contrast, without vpr, nuclear REAF increases at 120 minutes (~25%). Similar to the response to poly(I:C) in THP-1, cytoplasmic REAF expression increases within 30 minutes of infection with either virus (Figure 3I). Interestingly REAF cytoplasmic upregulation was even greater for HIV-1 89.6^{WT} than for the mutant virus without Vpr possibly reflecting exclusion from the nucleus. These results support the proposition that Vpr overcomes REAF restriction in MDMs where REAF expression is high and is induced further by viral replication. Figure 3J confirms that the HIV-1 $89.6^{\Delta vpr}$ virus used in these experiments is restricted to replication in MDMs when compared with the wild type

138 virus expressing Vpr (HIV-1 89.6^{WT}).

139 REAF has many properties of restriction factors (21, 22). It interacts with HIV-1 reverse
140 transcripts, impeding reverse transcription and integration (12). It is germline encoded,
141 constitutively expressed in cells, regulated by the proteasome system, suppressed by Vpr and
142 upregulated by poly(I:C).

143 IFNα induces many HIV restriction factors (23, 24). We used RNA-Seq to determine if
144 IFNα upregulated REAF mRNA in MDMs. Figure 4A shows IFNα induced upregulation of
145 antiviral genes, including HIV restriction factors APOBEC3G, IFITM1-3, MX2, tetherin and
146 Viperin (21) but with little or no upregulation of REAF mRNA. Further, there was no change in
147 either subcellular distribution or overall levels by Western blotting or image flow cytometry (a
148 slight increase by Western blotting was observed in some donors, Figure S3). Nor was REAF
149 mRNA or protein upregulated in $CD4^+$ T-cells (Figure S4) or in THP-1 in response to IFN α, β, or
150 γ (Figure S5).

151 Restriction factors are often under evolutionary positive selection at sites that interact with
152 virus. We found no evidence of positive selection of REAF in the primate lineage (Figure 4B) and
153 so it fits better with a model of purifying selection. This could reflect a role in G2/M progression,
154 precluding changes to its primary sequence. REAF is unlike the evolving HIV restriction factors
155 like APOBEC3G, SAMHD1, TRIM5 or BST2/tetherin and is more similar to SERINC3 and 5
156 which are not under positive selection (25, 26). We propose that REAF is a multi-functional
157 or 'moonlighting' protein with at least two cellular roles (27). In cycling T-cells, REAF is
158 associated with G2/M transition, so depletion of it by Vpr induces an accumulation in G2/M. In
159 non-cycling cells, Vpr is important for HIV infection of macrophages where REAF is highly
160 expressed.

Materials and methods:

Ethics Statement

Leucocyte cones from blood donors, from which PBMCs were isolated, were obtained from the NHS Blood Transfusion service, St. George's Hospital, London. Donors were anonymous and thus patient consent was not required. The local ethical approval reference number is 06/Q0603/59.

Cell lines

HEK-293T (ATCC), THP-1, C8166, HeLa-CD4 parental (all NIBSC AIDS Reagents) and shRNA-REAF (HeLa-CD4 shRNA-REAF, previously described) were maintained at 37°C in 5% CO_2 (10). Cells were grown in Dulbecco's Modified Eagle Medium (DMEM, ThermoFisher) supplemented with fetal bovine serum (5-10%, Thermo Fisher) and appropriate antibiotics. HeLa-CD4-shRNA-REAF were selected for resistance to puromycin in media supplemented with 10µg/ml puromycin.

Transfections and virus production

The infectious molecular clone for HIV-1 89.6 was obtained from the Centre for AIDS Research (NIBSC, UK). Infectious full-length and chimeric HIV clones were prepared by linear polyethylenimine 25K (Polysciences), Lipofectamine 2000 (Invitrogen) or Lipofectamine 3000 (Invitrogen) transfection of HEK-293T. Plasmid constructs HIV-1 89.6$^{\Delta vif}$, HIV-1 89.6$^{\Delta vpr}$ and HIV-1 89.6$^{\Delta vpu}$ were generated from the HIV-1 89.6 molecular clone, using overlap extension PCR *(24)*. Clones were confirmed by plasmid sequencing (Source BioScience). Primer sequences are available on request.

HEK-293T were plated at $2x10^4/cm^2$ in 8-well chamber slides (confocal microscopy), or 10cm dishes (virus production) 48 hours prior to transfection. For virus production, supernatant was harvested 72 hours post-transfection and cleared of cell debris by centrifugation at 500 x *g* for 5 minutes before storage at -80^0C. Mutant virus with low titer were amplified by C8166 for 48 hours before harvesting. HIV-1 89.6 (VSV-G) was generated by combining the transfer vector pCSGW with the envelope pMDG VSV-G and the core construct p8.91-89.6*gag* in HEK-293T as above and has been previously described *(12)*.

Titration of replication competent virus

HeLa-CD4 were seeded at 1.5×10^4 cells/well in 48-well plates to form an adherent monolayer of cells. Cell monolayers were challenged with serial 1/5 dilutions of virus and titre was assessed after 48 hours by *in situ* intracellular staining of HIV-1 p24 to identify individual foci of viral replication (FFU), as described previously *(12)*. For infection time course experiments, 400-500µl of 1×10^5 FFU/ml (HeLa-CD4) or 3×10^3 FFU/ml (MDMs) virus was added per well to cells cultured in 6-well trays for 24 hours (HeLa-CD4) or 7 days (for MDMs). In Figure 3J, cells were challenged with 50ng p24 in 6-well plates with 2×10^6 MDMs per well. Supernatants were harvested on days 0, 2, 8, 21 and 28 post challenge and p24 concentration analysed by ELISA.

cDNA synthesis and qPCR

Total RNA was extracted from MDMs using an RNeasy Plant Mini Kit (QIAGEN), and cDNA was synthesised with SuperScript™ III First-Strand Synthesis System (Invitrogen), according to manufacturer's instructions. cDNA was subjected to real-time quantitative PCR (qPCR) using

207 REAF, OAS1 and β-actin primer pairs with SYBR® Green detection of amplified transcripts
208 (QuantiTect SYBR Green PCR Kit, QIAGEN). Data acquisition and analysis were performed
209 using the ABI PRISM™ 7500 SDS software. Primer sequences are available upon request.

210

211 **Gene expression microarray**

212 Prior to microarray analysis, MDM RNA was prepared using the Illumina™ TotalPrep™ RNA
213 Amplification Kit (Ambion), according to manufacturer's instructions. The probes were
214 hybridised on an Illumina™ HT12v3 bead array following the manufacturer's standard
215 hybridisation and scanning protocols. Raw measurements were processed by GenomeStudio
216 software (Illumina), and quantile normalised. All microarray data are publicly available in the
217 Gene Expression Omnibus (GEO) database with accession number GSE54455.

218

219 **IFN, Poly(I:C) and treatment**

220 MDMs, $CD4^+$ T-cells and THP-1 were treated with IFN (100-500IU/ml, specified) for 24 or 48
221 hours (specified) before harvest for RNA extraction; analysis by Western blotting or imaging flow
222 cytometry. THP-1 were treated with poly(I:C) (25μg/ml, HMW/LyoVec™, Invitrogen) for 48
223 hours before analysis by Western blotting or imaging flow cytometry. Prior to IFN or poly(I:C)
224 treatment, THP-1 were treated with phorbol 12-myristate 13-acetate (PMA, 62 ng/ml) for 3 days
225 and then PMA-free DMEM for 2 days to allow differentiation and recovery. For Figure 4B and
226 Figure S4, recombinant IFNα was purchased from Sigma (Interferon-αA/D human Cat. No. I4401-
227 100KU) and is a combination of human subtypes 1 and 2. For Figure S3 and 5, recombinant human
228 IFNs are from Peprotech.

229

Western blotting

Cells were harvested and lysed in 30-50µl of radioimmunoprecipitation (RIPA) buffer supplemented with NaF (5µM), Na_2VO_3 (5µM), β-glycerophosphate (5µM) and 1x Protease Inhibitor Cocktail (Cytoskeleton). The protein concentration of each sample was determined using the BCA Protein Assay Kit (Pierce). 25µg or 12.5µg of total protein was separated by SDS-PAGE (4-12% Bis-Tris Gel, Invitrogen), at 130V for 1 hour 30 minutes in MOPS SDS Running Buffer (Invitrogen). Separated proteins were transferred onto nitrocellulose membrane (0.45µm pore size, GE Healthcare) at 45V for 2 hours, in ice-cold NuPAGE™ Transfer Buffer (ThermoFisher). Membranes were blocked for 1 hour at room temperature in 5% (w/v) non-fat milk powder in TBST buffer. Specific proteins were detected with primary antibodies by incubation with membranes overnight at 4^0C and with secondary antibodies for 1 hour at room temperature. All antibodies were diluted in blocking buffer. Proteins were visualised using ECL Prime Western Blotting Detection Reagent (GE Healthcare) and imaged using either ChemiDoc Gel Imaging System (Bio-Rad) or exposed to CL-XPosure films (ThermoScientific) and developed.

Antibodies

Primary rabbit polyclonal antibody to REAF (RbpAb-RPRD2) has been previously described (12). For imaging flow cytometry and confocal microscopy, RbpAb-RPRD2 was detected using goat anti-rabbit IgG conjugated with Alexa Fluor 647 (Invitrogen). FITC-labelled anti-phospho-histone H3 (Ser28) was used (BD Bioscience) for imaging flow cytometry and confocal microscopy. MsmAb-IFITM1 (clone 5B5E2, Proteintech), was detected by goat anti-mouse IgG Alexa Fluor 555 (ThermoFisher) for imaging flow cytometry, and by anti-mouse IgG antibody conjugated to HRP (GE Healthcare) for Western blotting, as were MsmAb-Mus81 and MsmAb-GFP (both

Abcam). Also for Western blotting, RbpAb-RPRD2, RbmAb-IFITM3 (EPR5242, Insight Biotechnology), RbpAb-GAPDH, RbpAb-βActin, RbmAb-phospho-histone H3 (Ser10/Thr11) and RbpAb-HLTF (all Abcam) were detected with secondary antibody: donkey anti-rabbit IgG conjugated to HRP (GE Healthcare).

Immunoprecipitation

HEK-293T, transfected with either VPR-GFP or GFP control expression vector, were lysed 72hrs post transfection in RIPA buffer supplemented with NaF (5µM), Na_2VO_3 (5µM), β-glycerophosphate (5µM) and 1x Protease Inhibitor Cocktail (Cytoskeleton). Total protein concentration was determined using BCA Protein Assay Kit (Pierce). GFP-TRAP® magnetic agarose beads were equilibrated in ice cold dilution buffer (10 mM Tris/Cl pH 7.5; 150 mM NaCl; 0.5 mM EDTA) according to manufacturer's instructions (Chromotek). Cell lysates containing 100µg of total protein were incubated with 10µl of equilibrated beads for 2 hours at 4ºC with gentle agitation. Beads were washed three times with PBST buffer before analysis by Western blotting.

Magnetic separation of primary human lymphocytes

Peripheral blood mononuclear cells (PBMCs) were isolated from leukocyte cones (NHS Blood Transfusion service, St. George's Hospital, London) by density gradient centrifugation with Lymphoprep™ density gradient medium (STEMCELL™ Technologies). Peripheral monocytes were isolated from PBMCs, using the human $CD14^+$ magnetic beads (Miltenyi Biotech) according to manufacturer's instructions. $CD4^+$ T-cells were isolated from the flow-through, using the human

276 $CD4^+$ T-cell isolation kit (Miltenyi Biotech). $CD14^+$ monocytes, and $CD4^+$ T-cells were either
277 differentiated, or fixed directly after isolation for intracellular staining. To obtain M1 and M2
278 macrophages (M1/M2 MDMs), monocytes were treated with either granulocyte-macrophage
279 colony stimulating factor (GM-CSF, 100ng/ml, Peprotech) or macrophage colony stimulating
280 factor (M-CSF, 100ng/ml) for 7 days, with medium replenished on day 4. To obtain dendritic cells
281 (DC), monocytes were treated with GM-CSF (50ng/ml) and IL-4 (50ng/ml) for 7 days, with
282 medium replenished on day 4. Activated $CD4^+$ T-cells were obtained by stimulating freshly
283 isolated $CD4^+$ T-cells at $1x10^6$/ml with T cell activator CD3/CD28 Dynabeads (ThermoFisher), at
284 a bead-cell-ratio of 1, for 7 days. Magnetic beads were removed prior to intracellular staining and
285 flow cytometry.
286
287 **Immunofluorescence**
288 Transfected cells were washed with PBS and fixed in 2% paraformaldehyde/PBS for 10 minutes,
289 at room temperature. Fixed cells were then permeabilised in 0.2% Triton-X100/PBS for 20
290 minutes, at room temperature. Cells were incubated with primary antibodies in PBS containing
291 0.1% Triton-X100 and 2% BSA overnight at 4^0C. After 3 washes in PBS, cells were then labeled
292 with secondary antibodies in the same buffer for 1 hour, at room temperature, and washed 3 times
293 with PBS. For confocal microscopy, nuclei were counterstained with Hoechst 33342 (2µM,
294 ThermoFisher) for 5 minutes, at room temperature. Labeled cells were mounted with ProLong™
295 Diamond Antifade Mountant (ThermoFisher) and analysed on a laser scanning confocal
296 microscope LSM 710 (Carl Zeiss). Images were acquired with ZEN software and analysed with
297 ImageJ.
298

299 **Imaging flow cytometry**

300 Cells were fixed in FIX&PERM® Solution A (Nordic MUbio) for 30 minutes, and permeabilised
301 with 0.2% Triton™-X 100/PBS. MDMs were blocked with human serum (1%). The staining buffer
302 used was: 0.1% Triton™-X 100 0.5% FCS. Nuclei were stained with DAPI (1µg/ml) for two hours.
303 Imaging flow cytometry was performed using the Amnis ImageStream®x Mark II Flow Cytometer
304 (Merck) and INSPIRE® software (Amnis). A minimum of 10,000 events were collected for each
305 sample, gating strategy is shown in Figure S6. IDEAS® software (Amnis) was used for analysis
306 and to determine the 'nuclear enrichment score'. The nuclear enrichment score is a comparison of
307 the intensity of REAF fluorescence inside the nucleus to the total fluorescence intensity of the
308 entire cell. A lower nuclear enrichment score indicates a lower proportion of overall REAF is
309 located within the nucleus.

310

311 **Statistics**

312 Statistical significance in all experiments was calculated by Student's t-test (two tailed). Data are
313 represented as mean ± standard deviation (error bars). GraphPad Prism and Excel were used for
314 calculation and illustration of graphs.

315

316 **Cell synchronisation**

317 HeLa-CD4 were synchronised at the G2/M border by nocodazole (200ng/ml) for 16 hours. Where
318 synchronised cells were infected with virus, an initial S phase block with thymidine (4mM) was
319 induced for 24 hours followed by a PBS wash and a treatment with nocodazole (100ng/ml) for a
320 further 16 hours. Collecting only those cells that were in suspension, as well as those that detached
321 easily with a manual "shake-off", enriched the population of mitotic cells.

322

323 **Cell cycle analysis**

324 Cell cycle phase distribution was determined by analysis of DNA content via either flow cytometry
325 (BD FACS Canto™ II) or imaging flow cytometry. Cells were fixed in ice-cold ethanol (70%),
326 treated with ribonuclease A (100µg/ml) and stained with propidium iodide (PI, 50µg/ml) or fixed
327 in FIX&PERM® Solution A (Nordic MUbio) and stained with DAPI (1µg/ml). Mitotic cells were
328 also identified by flow cytometry using the anti-phospho-histone H3 (Ser28) antibody. Cell lysates
329 were assessed by Western blotting using the anti-phospho-histone H3 (Ser10/Thr11) antibody as
330 an additional mitotic marker. Chromatin morphology and anti-phospho-histone H3 (Ser28) were
331 used to determine the cells in indicated phases of the cell cycle and mitosis in confocal microscopy
332 experiments.

333

334 **Evolutionary analysis**

335 To ascertain the evolutionary trajectory of REAF, we analysed DNA sequence alignments of
336 REAF from 15 species of extant primates using codeml (as implemented by PAML 4.2) (28). The
337 evolution of REAF was compared to several NSsites models of selection, M1, M7 and M8a
338 (neutral models with site classes of dN/dS <1 or ≤1) and M2, M8 (positive selection models
339 allowing an additional site class with dN/dS >1). Two models of codon frequencies (F61 and F3x4)
340 and two different seed values for dN/dS (ω) were used in the maximum likelihood simulations.
341 Likelihood ratio tests were performed to evaluate which model of evolution the data fit
342 significantly better. The p-value indicates the confidence with which the null model (M1, M7,
343 M8a) can be rejected in favor of the model of positive selection (M2, M8). The alignment of REAF
344 was analysed by GARD to confirm the lack recombination during REAF evolution (29). Neither

345 positively selected sites nor signatures of episodic diversifying selection were detected within
346 REAF by additional evolutionary analysis by REL and FEL or MEME (30).

347

348 **Data availibility**

349 All microarray data is available in the gene expression omnibus (GEO) database with accession
350 number GSE54455.

351

352

353

354

355

356

357

358

359

360

361

362

363

364

365

366

367

368

369

References (1-30):

1. Eckstein DA, Sherman MP, Penn ML, Chin PS, De Noronha CM, Greene WC, et al. HIV-1 Vpr enhances viral burden by facilitating infection of tissue macrophages but not nondividing CD4+ T cells. J Exp Med. 2001;194(10):1407-19.
2. Malim MH, Emerman M. HIV-1 accessory proteins--ensuring viral survival in a hostile environment. Cell Host Microbe. 2008;3(6):388-98.
3. Connor RI, Chen BK, Choe S, Landau NR. Vpr is required for efficient replication of human immunodeficiency virus type-1 in mononuclear phagocytes. Virology. 1995;206(2):935-44.
4. Heinzinger NK, Bukrinsky MI, Haggerty SA, Ragland AM, Kewalramani V, Lee MA, et al. The Vpr protein of human immunodeficiency virus type 1 influences nuclear localization of viral nucleic acids in nondividing host cells. Proc Natl Acad Sci U S A. 1994;91(15):7311-5.
5. Vodicka MA, Koepp DM, Silver PA, Emerman M. HIV-1 Vpr interacts with the nuclear transport pathway to promote macrophage infection. Genes Dev. 1998;12(2):175-85.
6. Balliet JW, Kolson DL, Eiger G, Kim FM, McGann KA, Srinivasan A. Distinct effects in primary macrophages and lymphocytes of the human immunodeficiency virus type 1 accessory genes vpr, vpu, and nef: mutational analysis of a primary HIV-1 isolate. Virology. 1994;200.
7. Chen R, Le Rouzic E, Kearney JA, Mansky LM, Benichou S. Vpr-mediated incorporation of UNG2 into HIV-1 particles is required to modulate the virus mutation rate and for replication in macrophages. J Biol Chem. 2004;279(27):28419-25.
8. Cohen EA, Terwilliger EF, Jalinoos Y, Proulx J, Sodroski JG, Haseltine WA. Identification of HIV-1 vpr product and function. J Acquir Immune Defic Syndr. 1990;3(1):11-8.
9. Bachand F, Yao XJ, Hrimech M, Rougeau N, Cohen EA. Incorporation of Vpr into human immunodeficiency virus type 1 requires a direct interaction with the p6 domain of the p55 gag precursor. J Biol Chem. 1999;274(13):9083-91.
10. Marno KM, O'Sullivan E, Jones CE, Diaz-Delfin J, Pardieu C, Sloan RD, et al. RNA-Associated Early-Stage Antiviral Factor Is a Major Component of Lv2 Restriction. J Virol. 2017;91(10).
11. Desai TM, Marin M, Sood C, Shi J, Nawaz F, Aiken C, et al. Fluorescent protein-tagged Vpr dissociates from HIV-1 core after viral fusion and rapidly enters the cell nucleus. Retrovirology. 2015;12:88.
12. Marno KM, Ogunkolade BW, Pade C, Oliveira NM, O'Sullivan E, McKnight A. Novel restriction factor RNA-associated early-stage anti-viral factor (REAF) inhibits human and simian immunodeficiency viruses. Retrovirology. 2014;11:3.
13. Romani B, Cohen EA. Lentivirus Vpr and Vpx accessory proteins usurp the cullin4-DDB1 (DCAF1) E3 ubiquitin ligase. Curr Opin Virol. 2012;2(6):755-63.
14. Laguette N, Bregnard C, Hue P, Basbous J, Yatim A, Larroque M, et al. Premature activation of the SLX4 complex by Vpr promotes G2/M arrest and escape from innate immune sensing. Cell. 2014;156(1-2):134-45.
15. Lahouassa H, Blondot ML, Chauveau L, Chougui G, Morel M, Leduc M, et al. HIV-1 Vpr degrades the HLTF DNA translocase in T cells and macrophages. Proc Natl Acad Sci U S A. 2016;113(19):5311-6.

16. Marechal A, Li JM, Ji XY, Wu CS, Yazinski SA, Nguyen HD, et al. PRP19 transforms into a sensor of RPA-ssDNA after DNA damage and drives ATR activation via a ubiquitin-mediated circuitry. Mol Cell. 2014;53(2):235-46.
17. Helmer RA, Martinez-Zaguilan R, Dertien JS, Fulford C, Foreman O, Peiris V, et al. Helicase-like transcription factor (Hltf) regulates G2/M transition, Wt1/Gata4/Hif-1a cardiac transcription networks, and collagen biogenesis. PLoS One. 2013;8(11):e80461.
18. Wei Y, Yu L, Bowen J, Gorovsky MA, Allis CD. Phosphorylation of histone H3 is required for proper chromosome condensation and segregation. Cell. 1999;97(1):99-109.
19. Groschel B, Bushman F. Cell cycle arrest in G2/M promotes early steps of infection by human immunodeficiency virus. J Virol. 2005;79(9):5695-704.
20. Balliet JW, Kolson DL, Eiger G, Kim FM, McGann KA, Srinivasan A, et al. Distinct effects in primary macrophages and lymphocytes of the human immunodeficiency virus type 1 accessory genes vpr, vpu, and nef: mutational analysis of a primary HIV-1 isolate. Virology. 1994;200(2):623-31.
21. Doyle T, Goujon C, Malim MH. HIV-1 and interferons: who's interfering with whom? Nat Rev Microbiol. 2015;13(7):403-13.
22. Kluge SF, Sauter D, Kirchhoff F. SnapShot: antiviral restriction factors. Cell. 2015;163(3):774- e1.
23. Goujon C, Malim MH. Characterization of the alpha interferon-induced postentry block to HIV-1 infection in primary human macrophages and T cells. J Virol. 2010;84(18):9254-66.
24. Cheney KM, McKnight A. Interferon-alpha mediates restriction of human immunodeficiency virus type-1 replication in primary human macrophages at an early stage of replication. PLoS One. 2010;5(10):e13521.
25. McLaren PJ, Gawanbacht A, Pyndiah N, Krapp C, Hotter D, Kluge SF, et al. Identification of potential HIV restriction factors by combining evolutionary genomic signatures with functional analyses. Retrovirology. 2015;12:41.
26. Murrell B, Vollbrecht T, Guatelli J, Wertheim JO. The Evolutionary Histories of Antiretroviral Proteins SERINC3 and SERINC5 Do Not Support an Evolutionary Arms Race in Primates. J Virol. 2016;90(18):8085-9.
27. Jeffery CJ. An introduction to protein moonlighting. Biochem Soc Trans. 2014;42(6):1679-83.
28. Yang Z. PAML 4: phylogenetic analysis by maximum likelihood. Mol Biol Evol. 2007;24(8):1586-91.
29. Kosakovsky Pond SL, Posada D, Gravenor MB, Woelk CH, Frost SD. GARD: a genetic algorithm for recombination detection. Bioinformatics. 2006;22(24):3096-8.
30. Pond SL, Frost SD. Datamonkey: rapid detection of selective pressure on individual sites of codon alignments. Bioinformatics. 2005;21(10):2531-3.

Acknowledgements: The monoclonal antibodies to HIV-1 p24 (EVA365 and 366) were provided by the EU Programme EVA Centre for AIDS Reagents, NIBSC, UK (AVIP Contract Number LSHP-CT-2004-503487). We thank Paul Clapham, Robin Weiss and Ari Fasatti for critical review of the manuscript.

Figure 1:

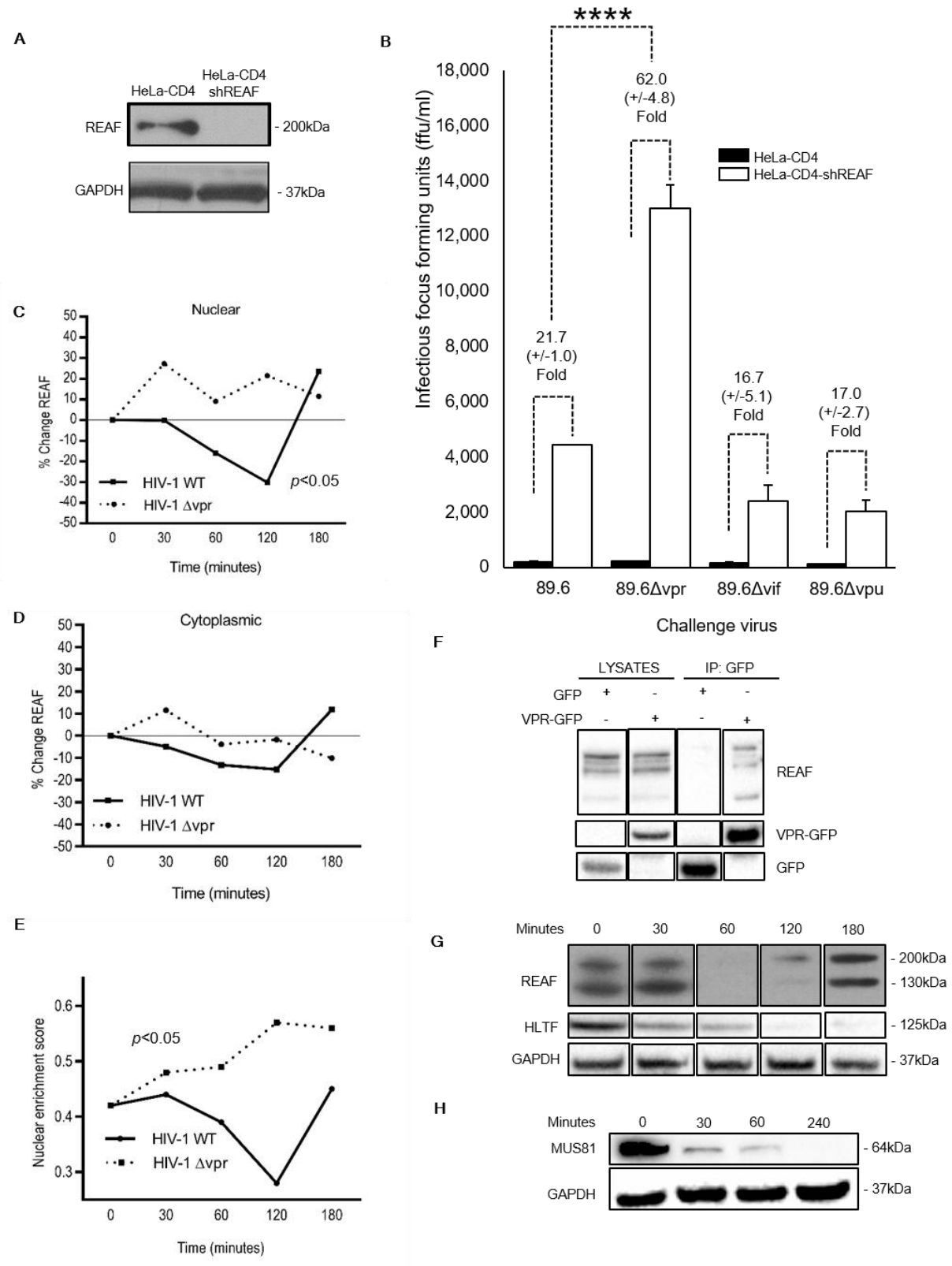

469

470

Figure 1: HIV-1 Vpr interacts with REAF and overcomes restriction. (A) REAF protein in HeLa-CD4 parental and HeLa-CD4 expressing shRNA targeting REAF (HeLa-CD4 shRNA-REAF). GAPDH is a loading control. **(B)** HeLa-CD4 shRNA-REAF challenged with HIV-1 89.6^{WT} or mutants HIV-1 $89.6^{\Delta vpr}$, $^{\Delta vif}$ or $^{\Delta vpu}$. HIV-1 $89.6^{\Delta vpr}$ is >60 fold more sensitive to REAF restriction than HIV-1 89.6^{WT} or other mutants. Input of approximately 50 FFU/ml on HeLa-CD4. Error bars indicate standard deviation and asterix indicate statistical significance (****=p<0.0001, Student's t-test). **(C-E)** Imaging flow cytometry measured mean fluorescence intensity (MFI) of REAF in the nucleus (C) and cytoplasm (D) of Hela-CD4 over time after challenge with HIV-1 89.6^{WT} or HIV-1 $89.6^{\Delta vpr}$. Results are representative of three separate experiments. A lower nuclear enrichment score (E) indicates a lower proportion of overall REAF is located in the nucleus (p<0.05). Statistical significance was calculated by Student's t-test. **(F)** Co-immunoprecipitated REAF was detected by Western blotting of VPR-GFP IP (right) but not GFP control IP (left). **(G)** Western blotting of REAF and HLTF in THP-1 over time post challenge with HIV-1 89.6^{WT}. GAPDH is a loading control. **(H)** Western blotting of MUS81 in Hela-CD4 over time post challenge with HIV-1 89.1^{WT}. GAPDH is a loading control.

471

472

473

474

475

476

Figure 2:

477

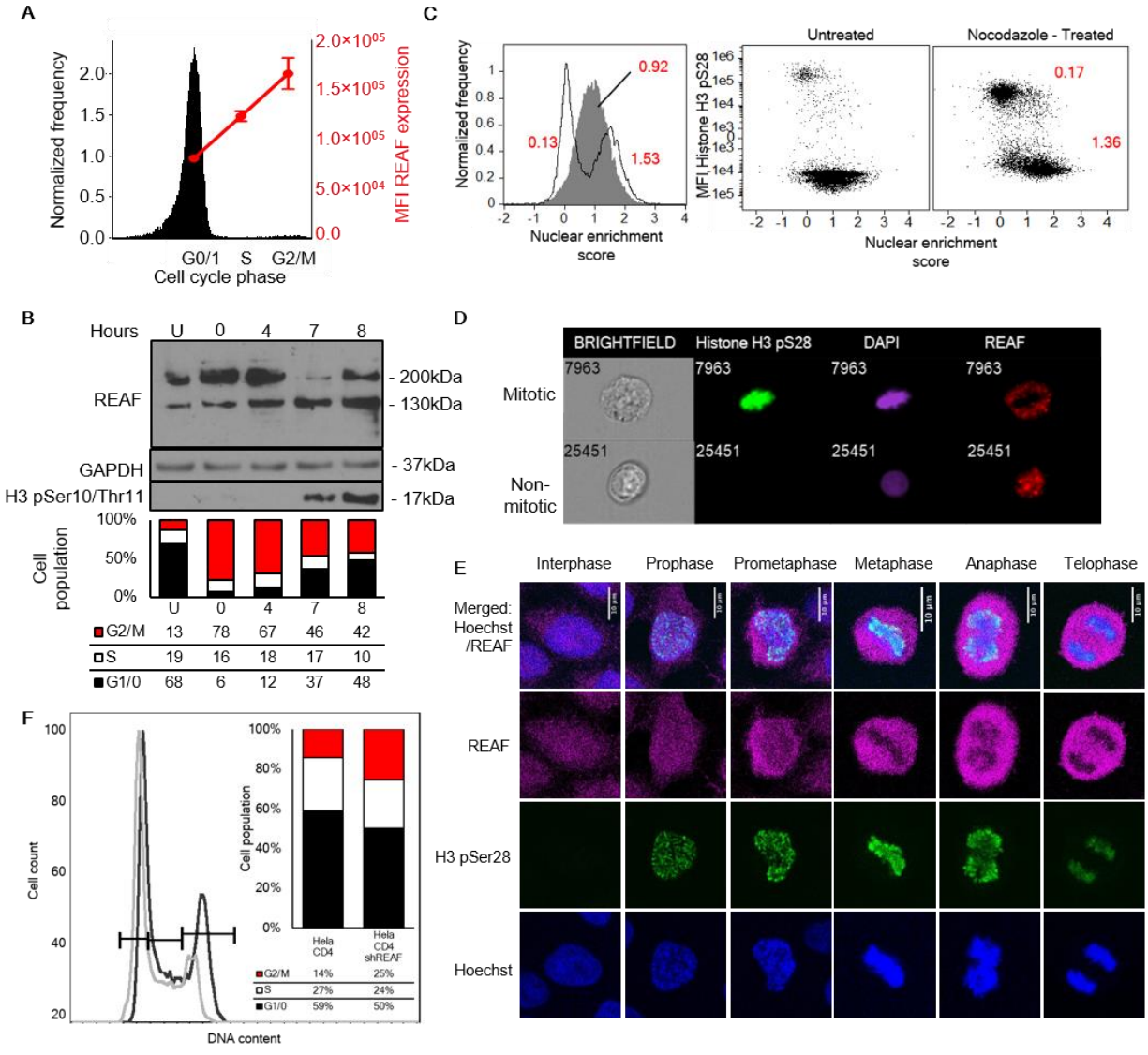

478

479

480

481

Figure 2: REAF expression fluctuates in the cell cycle and depletion results in cell accmulation G2/M. (A) Imaging flow cytometry of cell cycle phase and REAF expression in DAPI stained primary monocytes. **(B)** REAF expression in HeLa-CD4 over time after release from nocodazole induced cell cycle arrest. Phospho-histone H3 (Ser10/Thr11) is a mitotic marker and GAPDH is a loading control. Cell cycle profiles were determined and accompanying plots are in Figure S1. **(C-D)** Imaging flow cytometry of subcellular REAF in nocodazole treated HeLa-CD4. A lower nuclear enrichment score indicates a lower proportion of overall REAF in the nucleus - untreated: 0.92, nocodazole-treated: 0.13 (one population), 1.53 (another population) (left). Phospho-histone H3 (Ser28) staining confirmed mitotic cells had a lower score of 0.17 (right). Representative images (D) of subcellular REAF in mitotic and non-mitotic cells. **(E)** Confocal microscopy of subcellular REAF in HeLa-CD4. Phospho-histone H3 (Ser28) staining and chromatin morphology (Hoechst) were used for cell cycle phase identification. **(F)** Flow cytometry of cell cycle phase in PI stained HeLa-CD4 shRNA-REAF (black outline) and HeLa-CD4 (grey outline).

489

Figure 3:

490

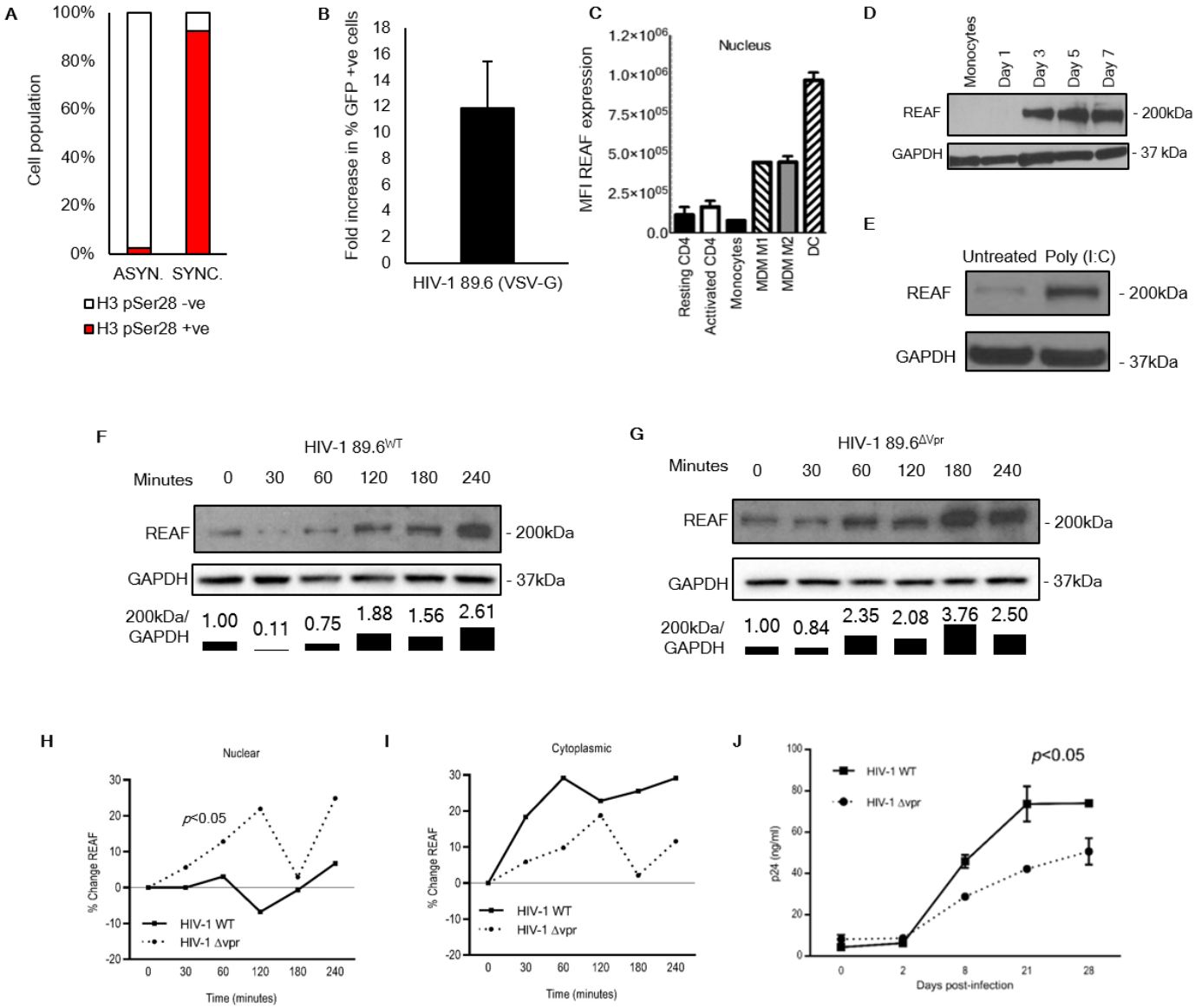

491

492

493

494

Figure 3: Mitotic cells are more susceptible to HIV-1 infection. Vpr down-modulates REAF in MDMs. (A, B) Thymidine/nocodazole treated HeLa-CD4 were released from cell cycle arrest at the G2/M border. After 2 hours of cycling into mitosis they, and untreated HeLa-CD4, were challenged in triplicate with HIV-1 89.6 (VSV-G) with a GFP reporter. Flow cytometry confirmed the synchronized population was significantly enriched for mitotic cells at the time of infection (identified using phospho-histone H3 (Ser28)) (A). Fold increase in viral infectivity was assessed 48 hours post challenge by flow cytometry. GFP fluorescence identified infected cells (B). (C) Nuclear expression of REAF in indicated cell types from two blood donors measured by imaging flow cytometry. (D) Western blotting of REAF expression during monocyte to macrophage differentiation with M-CSF. GAPDH is a loading control. (E) REAF protein in poly(I:C) treated, PMA differentiated, THP-1. GAPDH is a loading control. **(F, G)** MDMs were challenged with HIV-1 89.6^{WT} (F) or HIV-1 $89.6^{\Delta vpr}$ (G), harvested at indicated times post challenge, and analyzed for REAF expression. GAPDH is a loading control. Densitometric quantitation of 200kDa REAF is presented. **(H, I)** MDMs, challenged with HIV-1 89.6^{WT} or HIV-1 $89.6^{\Delta vpr}$, were analyzed by imaging flow cytometry for REAF expression in the nucleus (H) and cytoplasm (I) at the indicated times post challenge. (J) The infectivity of HIV-1 89.6^{WT} compared with HIV-1 $89.6^{\Delta vpr}$ in primary human macrophages. Viral input was equivalent at 50ng.

495

Figure 4:

A

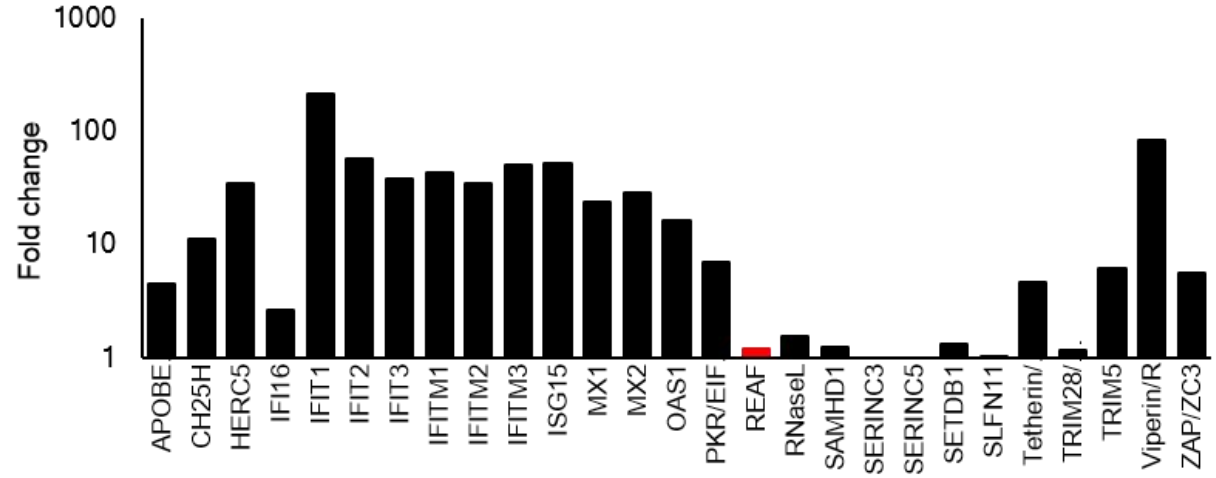

B

		M1 vs M2		M7 vs M8		M8a vs M8	
Codon freq. model	ω_o	2*ΔlnL	p-value	2*ΔlnL	p-value	2*ΔlnL	p-value
Fcodon	0.4	0.67	0.72	0.95	0.62	0.67	0.41
Fcodon	1.2	0.67	0.72	0.95	0.62	0.67	0.41
F3x4	0.4	0.53	0.86	0.53	0.77	0.32	0.57
F3x4	1.2	0.53	0.86	0.53	0.77	0.32	0.57

Figure 4: REAF is not IFN stimulated or under positive selection. (A) RNA-Seq determined change in REAF mRNA compared to other antiviral factors in MDMs treated with IFNα (500IU/ml). **(B)** REAF DNA sequences from 15 extant primate species (tree length of 0.2 substitutions per site along all branches of the phylogeny) (top) were analysed using the PAML package for signatures of positive natural selection (bottom). Initial seed values for ω (ω_O) and different codon frequency models were used in the maximum likelihood simulation. Twice the difference in the natural logs of the likelihoods (2*□InL) of the two models were calculated and evaluated using the chi-squared critical value. The p-value indicates the confidence with which the null model (M1, M7, M8a) can be rejected in favor of the model of positive selection (M2, M8).

507 **Supporting Information Figures 1 – 6:**

508

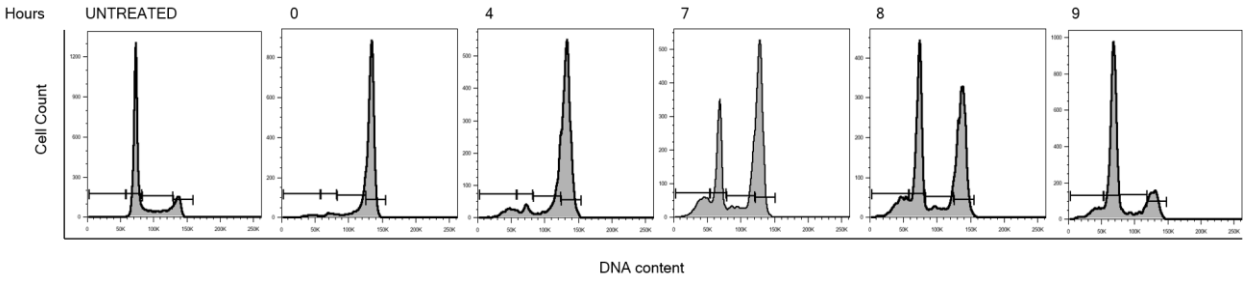

509

510

Fig. S1. Cell cycle flow cytometry plots accompanying Figure 2B. HeLa-CD4, synchronized at the G2/M border by treatment with nocodazole, were released from cell cycle arrest and allowed to cycle into mitosis. Cells, harvested over time after release and stained with DAPI, were analyzed for cell cycle phase by flow cytometry.

511

512

513

514

515

516

517

518

519

520

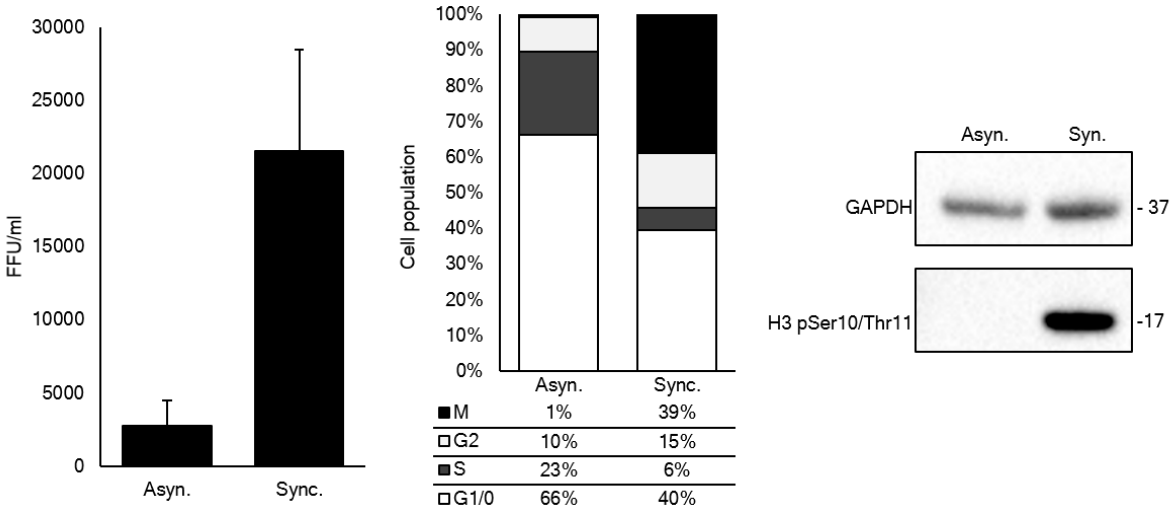

Fig. S2. Increased susceptibility of mitotic cells to HIV-1. HeLa-CD4, synchronized at the G2/M border by thymidine/nocodazole treatment, were released from cell cycle arrest and allowed to cycle synchronously into mitosis for 2 hours, at which point they were challenged with HIV-1 89.6^{WT}. Asynchronous, untreated HeLa-CD4 were simultaneously infected. Viral infectivity was assessed 48 hours after infection by intracellular staining of HIV-1 p24 to identify focus-forming units (FFUs)(left). Flow cytometry was used to determine cell cycle profiles of cells at the time of infection using DAPI stain to determine DNA content and anti-phospho-histone H3 (Ser28) antibody to identify mitotic cells (center). Western blotting was used to confirm an enriched population of mitotic cells in the synchronized population using phospho-histone H3 (Ser10/Thr11) as an alternative mitotic cell marker and GAPDH as a loading control (right).

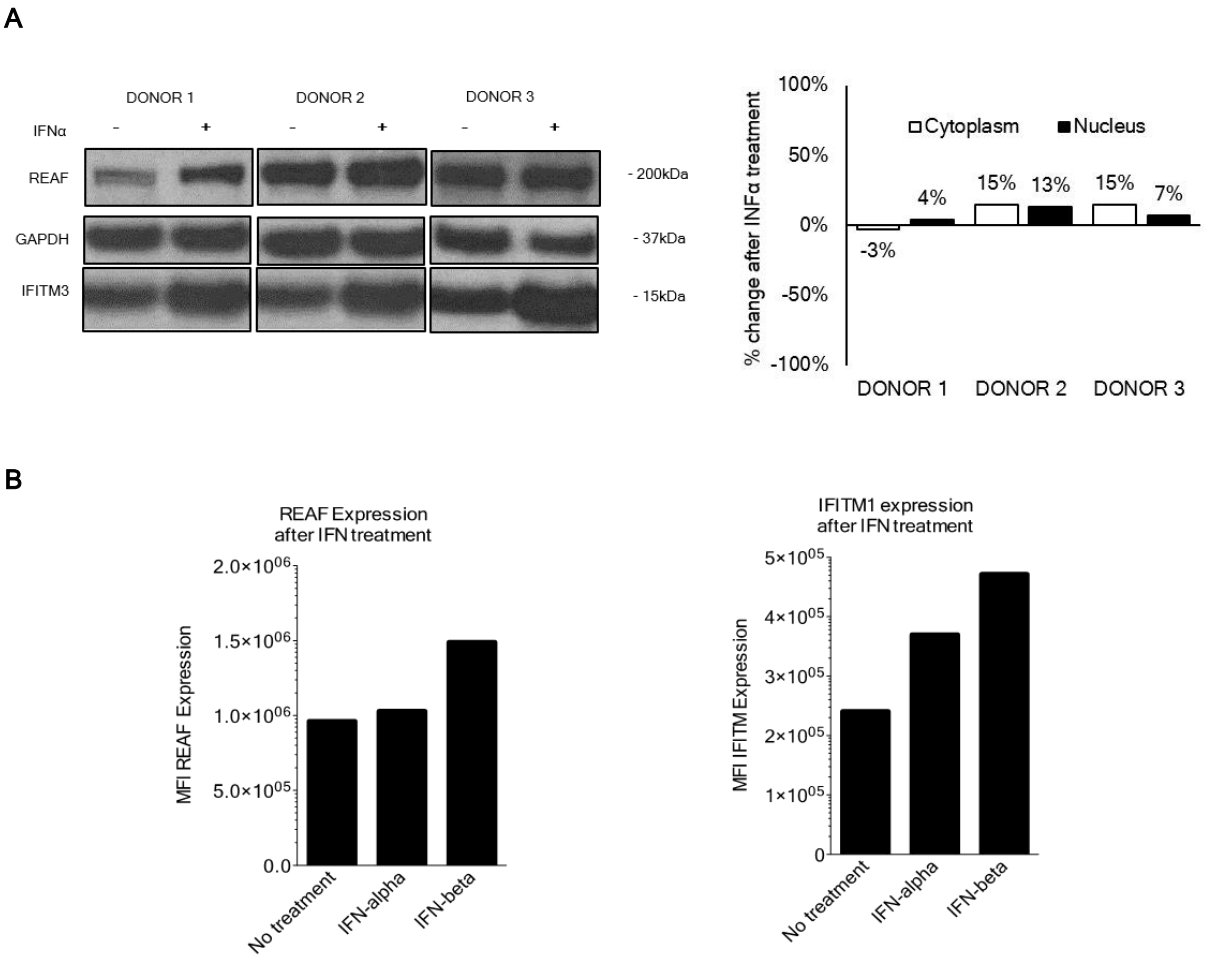

526

Fig. S3. No IFN induced increase in REAF protein expression or change in subcellular distribution in MDMs. (A) MDMs of three donors were treated with IFNα (100UI/ml) for 24 hours. Western blotting (left) and imaging flow cytometry (right) were used to determine REAF protein level and subcellular distribution with and without treatment. IFITM3 was used as a positive control for IFN induced protein upregulation and GAPDH as a loading control. **(B)** Imaging flow cytometry of REAF (left) and IFITM1 (right) expression in MDMs from a further donor treated with indicated IFNs (100UI/ml) for 24 hours. Expression of IFITM3 (right) was used as positive control for protein upregulation.

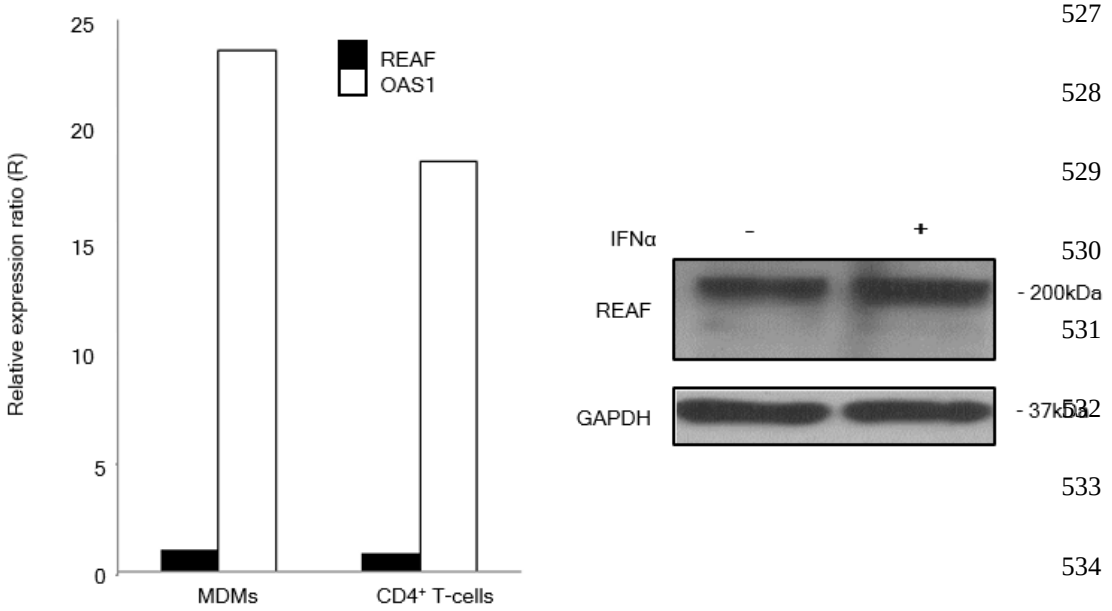

Fig. S4 No IFN induced upregulation of REAF mRNA in MDMs or CD4+ T-cells and no protein upregulation in CD4$^+$ T-cells. MDMs and primary CD4$^+$ T-cells were treated with IFNα (500IU/ml) for 48 hours. Increase in REAF mRNA, relative to that of β-actin, was measured by qPCR and OAS1 was used as a positive control for IFN induced upregulation (left). REAF protein expression (right) was also measured in CD4$^+$ T-cells by Western blotting with GAPDH as a loading control.

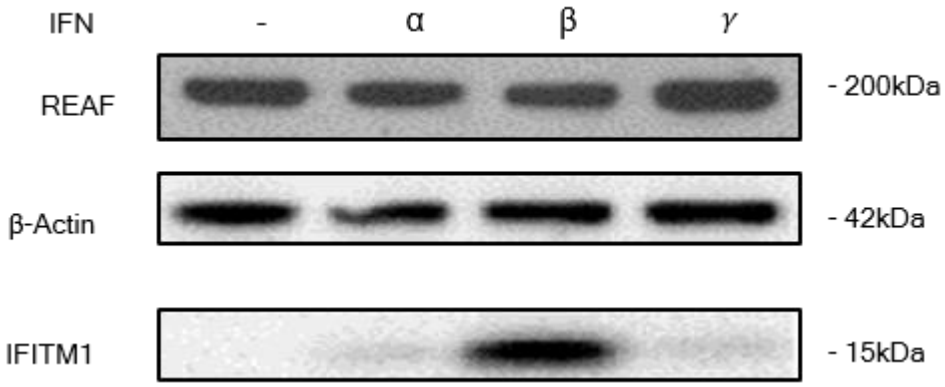

Fig. S5. No upregulation of REAF protein expression in IFN treated PMA differentiated THP-1. PMA differentiated THP-1 were analyzed by Western blotting after treatment with indicated IFNs (100IU/ml) for 24 hours. 200 and 80kDa bands are indicated, not all REAF bands are detected in all experiments. IFITM1 was used as a positive control for IFN induced protein upregulation and β-Actin as a loading control.

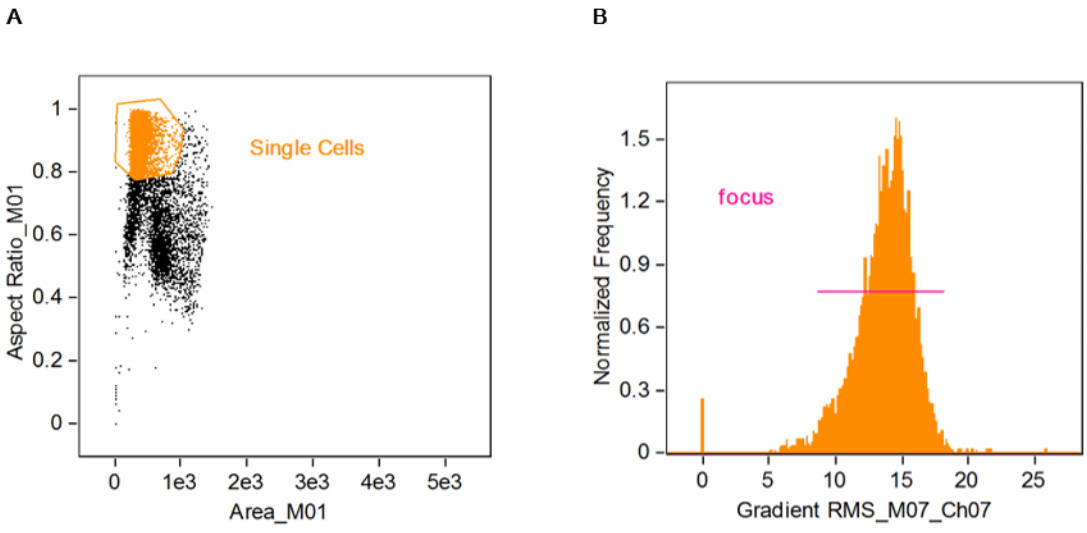

Fig. S6. Sequential gating strategy used in imaging flow cytometry analysis with IDEAS software. (A) Single cells were gated by area versus aspect ratio of the brightfield cell images. **(B)** Cells wih in focus images were gated by gradient RMS (root mean square of the rate of change of the image intensity profile). Representative plot examples are shown.